

Emergent topological phases in t_{2g} -orbital systems

Yuan-Yen Tai,¹ Cheng-Ching Joseph Wang,² Matthias J. Graf,² Jian-Xin Zhu,^{2,3} and C. S. Ting¹

¹*Texas Center for Superconductivity & Department of Physics,*

University of Houston, Houston, Texas 77004, USA

²*Theoretical Division & Center for Nonlinear Studies,*

Los Alamos National Laboratory, Los Alamos, New Mexico 87545, USA

³*Center for Integrated Nanotechnologies,*

Los Alamos National Laboratory, Los Alamos, New Mexico 87545, USA

(Dated: December 3, 2024)

Abstract

The electronic band structure of iron pnictides exhibits four Dirac cones, which are due to crystal symmetry and orbital bonding orientation. This hallmark signature presents the pnictide family as an ideal candidate in the search for quasi-two-dimensional topological crystalline insulators. In this report, we explore interaction-induced topological phases which cannot be described by conventional local order parameters. Based on a model Hamiltonian our symmetry analysis shows that spontaneous novel topological phases may be realized in compounds with tetragonal crystal field symmetry, where the electrons occupy the two degenerate t_{2g} energy levels at low temperature. We identify two stable topological phases in the ground state, which emerge from spontaneous orbital current order. These currents are driven by electronic correlations caused by inter-orbital Coulomb interactions. The first topological phase is an anomalous orbital Hall phase, characterized by a nonzero Chern number, while the second topological phase has a vanishing Chern number, though with an extra Z_2 -like invariant that preserves parity. More specifically, the interaction-induced novel phase of the quasi-two-dimensional topological crystalline insulator is protected by mirror reflection symmetries and therefore may be realized in pnictides.

PACS numbers: 71.10.Fd, 71.10.Pm, 73.20.-r

The class of topological insulators (TIs) is characterized by topological properties in the electronic wave function with the emergence of protected edge or surface states. In fact, the integer quantum Hall insulator is the first known TI, which was characterized by the topological Chern number [1] under the condition of broken time-reversal (TR) symmetry due to external magnetic fields. Haldane showed [2] that such a Chern insulator can be realized on a honey-comb lattice with opposite spontaneous internal magnetic fields between two different sub-lattices, even in the absence of external magnetic fields. By promoting Haldane's model to the class of Hamiltonians with spin degrees of freedom that respect the TR symmetry in the presence of strong spin-orbit coupling (SOC), the quantum-spin Hall insulator, characterized by a nontrivial Z_2 topological invariance, was proposed [3]. Later this idea was generalized to TIs with Z_2 symmetry in three dimensions (3D). One of the non-trivial topological properties that usually accompanies TIs is an odd number of Dirac cones of the edge or surface states in the edge or surface Brillouin zone. Experimentally, the quantum-spin Hall insulator was realized in the quasi-two-dimensional (quasi-2D) sub-bands of HgTe/CdTe quantum wells [4], following the proposal by Bernevig and collaborators [5] based on strong SOC due to the heavy tellurium atom. Shortly thereafter the 3D-TI with Z_2 symmetry was realized in doped $\text{Bi}_{1-x}\text{Sb}_x$ alloys [6] and other predicted bismuth- and tellurium-based compounds [8–10].

The quest for topological phases in multi-orbital systems has also been pursued in cold atom gases and photonic crystals [11, 12]. However, there are few studies of multi-orbital systems in real solids beyond those with the honey-comb lattice as building block. Recently, the topological Kondo insulator in rare-earth materials attracted much attention [13], due to the hybridization of itinerant electrons with localized spins giving rise to odd parity under inversion. Since then topological crystalline insulators (TCIs) with even number of Dirac cones in the surface states were predicted for 3D semiconductors[14] and transition-metal oxides[15] due to the mirror symmetry of the crystal instead of the TR symmetry.

Here we propose a new route to realizing non-trivial emergent topological phases through Coulomb interactions within the t_{2g} low-energy manifold comprised of the d_{xz} and d_{yz} orbitals in correlated electron systems. It is well known that the degeneracy of the five $3d$ orbitals is lifted by a crystal field with cubic symmetry. The orbital manifold is split into triple degenerate, lower t_{2g} and double degenerate, upper e_g energy levels. In addition, under a tetragonal lattice distortion, which can occur in iron pnictides, the low-lying t_{2g} level can split even further into double degenerate, lower d_{xz}/d_{yz} and upper d_{xy} levels and vice versa[16]. In contrast to the requirement

of strong SOC in 3D-TIs, moderate and plausible electronic interactions are sufficient for achieving 2D interaction-induced TCIs. We show that non-trivial topological phases can be induced by generating spontaneous orbital currents in a spinless low-energy two-orbital model with t_{2g} symmetry, which can lead to the anomalous orbital Hall (AOH) effect. Consequently, this effect offers an alternate path for the realization of the topological Mott insulator [18]. We note that the nature of these orbital currents is different from the loop or current flux phases that were employed to describe the pseudo-gap phase in the copper-oxide superconductors [17, 19–21], which have different orbital degrees of freedom, crystal symmetries, and conduction band topology.

Based on our studies, one may construct two degenerate mean-field ground state configurations from the d_{xz} and d_{yz} orbitals, which respects the σ_v spatial symmetry (see Supplementary Section I and II). The type **I** configuration [11, 12], which is frequently discussed in the literature, is the $d_{xz/yz}$ orbital-locked orientation of the nearest neighbor (NN) chemical bond direction. On the other hand, the type **II** configuration is the $d_{xz/yz}$ orbital-locked orientation of the next-nearest neighbor (NNN) chemical bond direction. Indeed, as will become clearer later, it is the type **II** configuration that is responsible for the generation of spontaneous orbital currents in the mean-field ground state with topologically non-trivial phases.

Since transition-metal compounds with crystal-field splitting and tetragonal lattice distortion have the d_{xz} and d_{yz} orbitals occupy the double degenerate ground state of the split t_{2g} manifold, we begin our detailed study with a spinless two-orbital Hamiltonian model [3, 4, 24], which successfully reproduced the electronic structure of the 122 iron pnictides in itinerant limit. Within mean-field theory of the correlated electron Hamiltonian, spontaneous orbital current order can be induced by inter-orbital Coulomb interaction. The orbital order gaps out the Dirac dispersion in the bulk bands and generates two edge bands with linear dispersion in one quarter of the Brillouin zone (BZ). This generates a one-dimensional (1D) version of two Dirac cones for spinless or spin polarized fermions. When further extending the model to the spinful Hamiltonian with spin degrees of freedom, we can discuss two uniquely distinguishable phases: In phase **I**, \uparrow / \downarrow spin has identical spin Chern number with the Chern number for occupied bands, $\mathcal{C} = |\mathcal{C}_\uparrow + \mathcal{C}_\downarrow| = 4$, whereas in phase **II**, the \uparrow / \downarrow spin has opposite spin Chern number with the vanishing Chern number, $\mathcal{C} = \mathcal{C}_\uparrow + \mathcal{C}_\downarrow = 0$. We observe that phase **I** and the spinless Hamiltonian are a direct realization of the Chern insulator, while phase **II** leads to the interaction-induced topological crystalline insulator (TCI) protected by mirror symmetry. Without the introduction of additional terms, the mean-field calculation shows that both states of phase **I** and **II** are degenerate. Introducing an on-

site intra-orbital spin-exchange interaction lifts this degeneracy and phase **II** becomes eventually the ground state.

THE SPINLESS FERMION MODEL

We start with a two-orbital model Hamiltonian for spinless fermions to facilitate our symmetry analysis and discussion,

$$\begin{aligned}\hat{H} = & \sum_{I \neq J, \alpha \beta} t_{IJ}^{\alpha\beta} c_{I\alpha}^\dagger c_{J\beta} + i \lambda_{AOH} \sum_{I \neq J, \alpha \neq \beta} \epsilon_{IJ}^{\alpha\beta} c_{I\alpha}^\dagger c_{J\beta} \\ & + \lambda_0 \sum_{I\alpha} (-1)^\alpha c_{I\alpha}^\dagger c_{I\alpha} + i \lambda_1 \sum_{I, \alpha \neq \beta} (-1)^\alpha c_{I\alpha}^\dagger c_{I\beta} \\ & - \sum_{I\alpha} \mu c_{I\alpha}^\dagger c_{I\alpha},\end{aligned}\tag{1}$$

where I, J are site indices, $\alpha, \beta \in [1, 2]$ are orbital indices. $\epsilon_{IJ}^{\alpha\beta}$ describe the inter-orbital current term as shown in Fig. 1(a) and their values are given in Table I of the SM. The first term with hopping parameter $t_{IJ}^{\alpha\beta}$ is the kinetic term of spinless fermions in the lattice and μ is the chemical potential. The AOH effect is described by the complex hopping term between different orbitals for sites I and J with the spinless coupling constant λ_{AOH} determined by spontaneously generated current through the inter-orbital Coulomb interaction. The on-site orbital energy difference λ_0 is responsible for the on-site orbital charge polarization, which can be induced by external electric field parallel to the lattice and the on-site complex hopping with coupling constant λ_1 describes the on-site inter-orbital coherence.

In the case of translational invariant crystal symmetry, the spinless Hamiltonian can be reduced to 2×2 matrix form in \mathbf{k} -space, that is, $\hat{H}(\mathbf{k})$, with basis functions $\psi_{\mathbf{k}} = (c_{\mathbf{k}\alpha}, c_{\mathbf{k}\beta})^T$ (where T is the transpose operation). We derive the expression $\hat{H}(\mathbf{k}) = E_0(\mathbf{k}) + \vec{B}(\mathbf{k}) \cdot \vec{\tau}$, where $\vec{B} = (X, Y, Z)$ and $\vec{\tau} = (\tau_x, \tau_y, \tau_z)$ are the Pauli matrices. The ancillary functions X, Y and Z are given in the SM. The diagonalization of $\hat{H}(\mathbf{k})$ attains the eigenvalues $E_{\pm}(\mathbf{k}) = E_0(\mathbf{k}) \pm B(\mathbf{k})$, where $B = |\vec{B}|$. The corresponding eigenvectors are

$$\begin{aligned}|+, \mathbf{k}\rangle &= (Z + B, X + iY)^T / \sqrt{2B^2 + 2ZB}, \\ |-, \mathbf{k}\rangle &= (-X + iY, Z + B)^T / \sqrt{2B^2 + 2ZB}.\end{aligned}\tag{2}$$

We find that Dirac cones exist in the dispersion of the bulk material when all interaction-induced terms and orbital polarization are turned off ($\lambda_{AOH} = \lambda_0 = \lambda_1 = 0$). Their positions are located

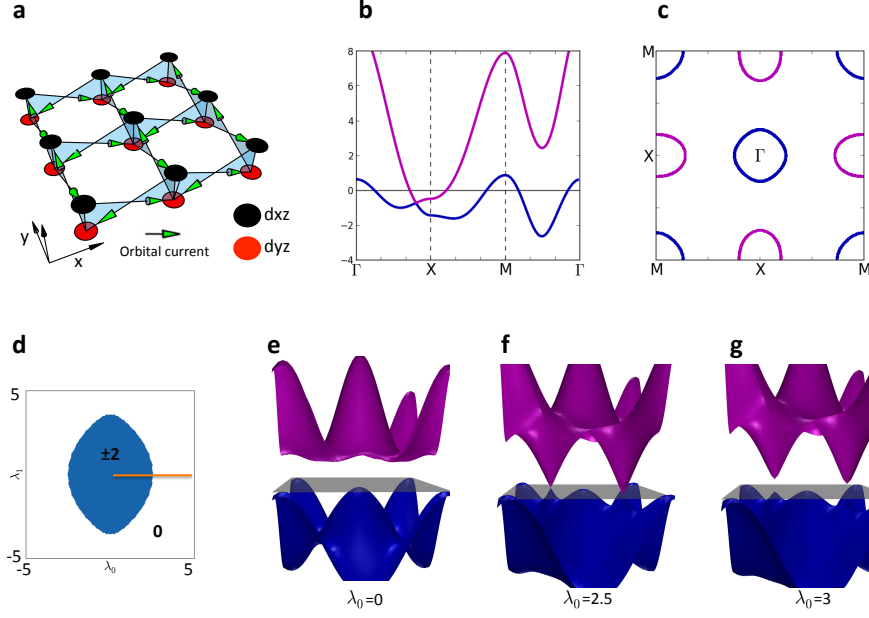


FIG. 1: Inter-orbital currents, electronic structure and phase diagram. **a**, The schematics of the orbital current order with inter-orbital Coulomb coupling λ_{AOH} . The coordinates x and y are in the 1-Fe per unit cell. **b** and **c**, the band structure and Fermi surfaces of the noninteracting Hamiltonian at half filling. **d**, The calculated phase diagram based on the Chern number \mathcal{C} with $\lambda_{AOH} = 1$. **e**, **f**, **g**, The evolution of the corresponding band structure from the TCI to metal to trivial band insulator as function of λ_0 at $\lambda_1 = 0$ along the orange line shown in the phase diagram of **(d)**.

at the k_x and k_y axes as determined by $B(\mathbf{k}) = 0$, see Fig. 1(b). In the following, we will focus on the situation with band topology inherited from $X\tau_x$ and $Y\tau_y$ terms, which is responsible for the topological phases when spin degrees of freedom are included in next section. The Hamiltonian $\hat{H}(\mathbf{k})$ with finite X and Y , and vanishing Z still preserve four Dirac cones but the location of the cones are moved to each quarter of BZ, $k = (\pm\frac{\pi}{2}, \pm\frac{\pi}{2}), (\pm\frac{\pi}{2}, \mp\frac{\pi}{2})$. When we turn on the $Z\tau_z$ term, these Dirac cones are gapped due to the σ_v symmetry breaking.

TOPOLOGICAL PHASES

In Fig. 1b and 1c we show the dispersion of the electronic band structure of the noninteracting bulk material at half filling when $\lambda_{AOH} = \lambda_0 = \lambda_1 = 0$. The Chern number of an occupied band can be calculated directly through the Berry curvature $\Omega^n(\mathbf{k})$ of the Hamiltonian $\hat{H}(\mathbf{k})$, which is defined as $\mathcal{C}_n(\lambda_{AOH}; \lambda_0; \lambda_1) = \frac{1}{2\pi} \int_{\mathbf{k} \in \text{BZ}} dk_x dk_y \Omega^n(\mathbf{k})$, with integer band index n , where the expression of $\Omega^n(\mathbf{k})$ is defined in the SM. The first observation is that $\mathcal{C}_n(\lambda_{AOH}; 0; 0) = \pm 2$ for

any real but nonzero λ_{AOH} . The second observation is that the sign of \mathcal{C}_n depends on the sign of λ_{AOH} , which determines the class of the Chern insulator, $\text{sign}(\mathcal{C}_n) = \text{sign}(\lambda_{AOH} \times (-1)^n)$, and the opposite orientation of the orbital currents in two bands. Since the topological phase with $\mathcal{C}_n = \pm 2$ is robust against weak perturbations by symmetry breaking terms, we show its stability region in the λ_0 - λ_1 phase diagram in Fig. 1d for moderately strong $\lambda_{AOH} = 1$. Note that the TI phase is induced by interaction and therefore vanishes for $\lambda_{AOH} \rightarrow 0$. Following the orange line in the phase diagram, we monitor the evolution of the bulk band gap as it closes and reopens with increasing λ_0 , see Figs. 1e to 1g. This leads to a sequence of phase transitions from topological Chern insulator to metal (around $\lambda_0 = 2.5$) and on to trivial band insulator with $\mathcal{C}_n = 0$.

THE SPINFUL FERMION MODEL

In materials with magnetic interactions, we need to consider electrons as fermions with spin degrees of freedom. Therefore, we promote the spinless two-band orbital model to the spinful model as $\hat{H}_s = \hat{H}_\uparrow[\epsilon_\uparrow] + \hat{H}_\downarrow[\epsilon_\downarrow]$. Here the sign of the orbital current direction is denoted as $\lambda_{AOH}^\sigma = \epsilon_\sigma \lambda_{AOH}$, where $\lambda_{AOH} > 0$ and $\epsilon_\sigma = \pm 1$ for each spin index $\sigma \in [\uparrow, \downarrow]$. A detailed analysis of the Hamiltonian \hat{H}^s reveals the following stable topological phases:

- **Phase I:** $\epsilon_\uparrow = \epsilon_\downarrow$ with Chern number $\mathcal{C} = \pm 4$ ($\mathcal{C}_\uparrow = \mathcal{C}_\downarrow$),
- **Phase II:** $\epsilon_\uparrow = -\epsilon_\downarrow$ with Chern number $\mathcal{C} = 0$ ($\mathcal{C}_\uparrow = -\mathcal{C}_\downarrow$).

For phase **I**, we find that the Chern number $\mathcal{C} = \pm 4$ for occupied bands is twice that for the spinless case due to the twofold degeneracy of spins. Here degenerate spins share the same orbital current direction. For phase **II**, we find that the Chern number classification scheme is insufficient to capture the topological nontrivial insulator phase. To see whether phase **II** is protected by band topology, we plot the edge states of the slab geometry in Fig. 2a. The calculated edge states along the (1,0,0) direction show two Dirac cones at $k_x = \pm \frac{\pi}{2}$. Furthermore, we show that these edge states are robust against the perturbation λ_1 up to a critical value of roughly 3, although the position of the Dirac cones are shifted away from $k_x = \pm \frac{\pi}{2}$ (see for example in Fig. 2b for $\lambda_1 = 2$). One may tend to claim that phase **II** is a conventional Z_2 quantum-spin Hall insulator, since the TR symmetry is respected by the mean-field Hamiltonian for phase **II** with $\mathcal{C} = 0$. However, it cannot be reconciled with the fact that the number of pairs of degenerate edge states is even instead of odd, as is the case for quantum spin-Hall insulator. Consequently, we claim that phase **II** is a quasi-2D TCI protected by mirror reflection symmetries as indicated by the even mirror

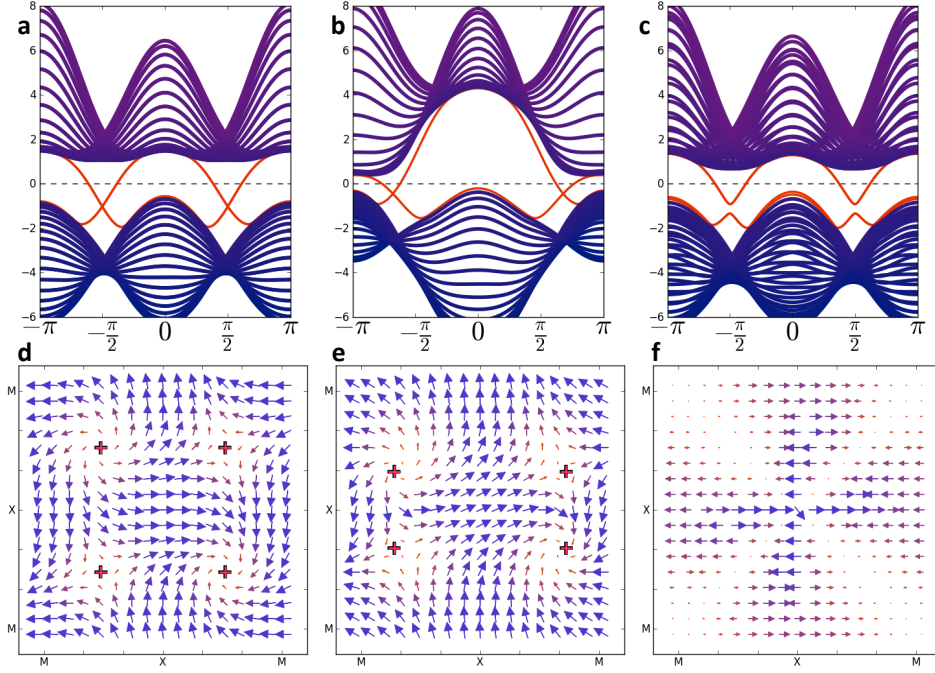


FIG. 2: **Band structure, edge states and vector plots of Pfaffian.** **a-c**, The electronic dispersion of the edge states (red lines) for different interaction parameters, but fixed Coulomb coupling $\lambda_{AOH} = 1$. **a**, TCI with $\lambda_0 = \lambda_1 = \lambda_R = 0$; **b**, TCI with $\lambda_1 = 2$, $\lambda_0 = \lambda_R = 0$; **c**, Band insulator with $\lambda_R = 0.03$, $\lambda_0 = \lambda_1 = 0$. Note that any finite Rashba coupling λ_R splits the Dirac cones. **d-f**, The corresponding vector plots of the complex Pfaffian function $\mathcal{P}(\mathbf{k})$. The bi-color code represents small (orange) to large (blue) modulus of $|\mathcal{P}(\mathbf{k})|$. The red crosses mark the positions of the vortex cores, i.e., Dirac cones where $\mathcal{P}(\mathbf{k}) = 0$. We used 20 lattice sites for the width of strip and 100 k -points in along the strip direction.

Chern number \mathcal{C}_M [28, 29] which is related to the spin Chern number of the occupied band with spin up/down $\mathcal{C}_{\uparrow,\downarrow}$ and given by $|\mathcal{C}_M| = |(\mathcal{C}_i - \mathcal{C}_{-i})/2| = |(\mathcal{C}_{\uparrow} - \mathcal{C}_{\downarrow})/2| = [2 - (-2)]/2 = 2$ (in the absence of SOC) as opposed to the Z_2 quantum-spin Hall insulator in the Kane-Mele lattice model with odd mirror Chern number $\mathcal{C}_M = 1$. In the next section, we propose a topological invariant for the TCI realized in phase **II**.

Notice that we only considered the imaginary part of the inter-orbital current order given by the λ_{AOH}^σ term, which is induced by the off-site Coulomb interaction. In general, one should include the real part too, however, since the real part of the term only causes a renormalization of hopping terms, it does not affect the band topologies of the phases and can be neglected in our discussion (for details see the SM). In addition, based on our model calculations, the phases **I** and

II are degenerate within numerical accuracy if we consider only the off-site Coulomb interaction. However, if an additional on-site intra-orbital spin-exchange term J is included the degeneracy between phases **I** and **II** is lifted and phase **II** assumes the lower energy (see Supplementary Section I).

MIRROR TOPOLOGICAL INVARIANT

The spinful mean-field Hamiltonian of phase **II** respects the TR symmetry. However, the number of Kramer's pairs at the edges is even instead of odd. Hence the number of Dirac cones is even, contrary to conventional TIs. This indicates that phase **II** is not adiabatically connected to the Z_2 symmetry of the quantum-spin Hall insulator, which is protected by the TR symmetry. We notice that the spinful Hamiltonian \hat{H}_s of phase **II** satisfies the mirror symmetry $\mathbf{M}\hat{H}_s(k_x, k_y)\mathbf{M}^{-1} = \hat{H}_s(k_x, -k_y)$, in which the mirror operator is given by $\mathbf{M} = \mathbf{P} \otimes \mathbf{T} = (\tau_x \mathbf{K}) \otimes (-i\sigma_y \mathbf{K})$ (see the SM for a detailed symmetry analysis). The operator \mathbf{K} performs the complex conjugation identical to the TR operation for spinless fermions. The generalized parity operator \mathbf{P} swaps two orbitals, while $-i\sigma_y$ is responsible for the spin flip under the TR operation \mathbf{T} . Because the mean-field Hamiltonian \hat{H}_s is invariant under the mirror symmetry \mathbf{M} , we define two orthogonal subspaces of Bloch wave functions $|u_n(\mathbf{k})\rangle$ in the BZ, which differ in their properties under mirror reflection: (1) the even parity subspace, spanned by $|u_n(\mathbf{k})\rangle$, is equivalent to $\mathbf{M}|u_n(\mathbf{k})\rangle$ up to a phase factor, and (2) the odd parity subspace, which is orthogonal to the former.

Analogous to the Z_2 symmetry in the Kane-Mele model of the quantum-spin Hall insulator [3], we introduce a mirror-invariant Pfaffian to capture the Z_2 -like “even/odd parity” of the spinful Hamiltonian $\hat{H}_s(\mathbf{k})$. Specifically, we define the mirror-invariant Pfaffian to measure the band topology of the quasi-2D TCI as

$$\mathcal{P}(\mathbf{k}) \equiv Pf[\langle u_m(\mathbf{k}) | \mathbf{M} | u_n(\mathbf{k}) \rangle], \quad (3)$$

where $|u_m(\mathbf{k})\rangle, |u_n(\mathbf{k})\rangle$ are two occupied orthogonal eigenstates of the Hamiltonian $\hat{H}_s(\mathbf{k})$. In the case of \mathbf{k} points belonging to the “even parity” subspace, i.e., along the k_x and k_y axes, the commutation relation $[\mathbf{M}, \hat{H}_s(\mathbf{k})] = 0$ holds. Therefore, the two eigenstates $|u_m(\mathbf{k})\rangle = \mathbf{M}|u_n(\mathbf{k})\rangle$ and $|u_n(\mathbf{k})\rangle$ are degenerate. As a result, the absolute value of the Pfaffian $\mathcal{P}(\mathbf{k})$, with \mathbf{k} along the k_x and k_y axes is unity, $|\mathcal{P}(\mathbf{k})| = 1$. On the other hand, \mathbf{k} points in the “odd parity” subspace satisfy the anti-commutation relation $\{\mathbf{M}, \hat{H}_s(\mathbf{k})\} = 0$. Here the mirror operation $\mathbf{M}|u_n(\mathbf{k})\rangle$ turns

occupied into unoccupied eigenstates, which are orthogonal eigenstates $|u_m(\mathbf{k})\rangle$ with vanishing Pfaffian $\mathcal{P}(\mathbf{k}) = 0$.

In Fig. 2d we show the calculated Pfaffian in the BZ of the TCI. We note four vortices, i.e., Dirac cones in the edge states, which are well separated by the "even parity" subspace along the k_x and k_y axes. An important question to address is how robust are these topological states. For that purpose, we examine the effects on the Pfaffian $\mathcal{P}(\mathbf{k})$ when an infinitesimally small mirror symmetry breaking interaction is adiabatically turned on. So let us introduce an on-site Rashba spin-orbit interaction $i\lambda_R \sum_{I\alpha\sigma} (-1)^\alpha (-1)^\sigma c_{I\alpha\sigma}^\dagger c_{I\alpha\bar{\sigma}}$. The corresponding Rashba Hamiltonian, written in momentum space as $\hat{h}_R(\mathbf{k}) = \lambda_R \tau_z \otimes \sigma_y$, breaks the mirror symmetry because it does not commute with \mathbf{M} in any where of the BZ, i.e., $[\mathbf{M}, \hat{H}_s(\mathbf{k}) + \hat{h}_R(\mathbf{k})] \neq 0$. This symmetry breaking field will destroy the mirror topological phase even though the interaction $\hat{h}_R(\mathbf{k})$ is infinitesimal. As we expect, the four vortices (Dirac cones) disappear for any nonzero Rashba spin-orbit interaction as shown in Fig. 2f. Consequently, an infinitesimal λ_R destroys the degeneracy of edge states and the previously gapless (crossing) edge states become gapped, see Fig. 2c.

A completely different scenario occurs when the local inter-orbital coupling $\lambda_1 \tau_y$, which preserves the mirror symmetry but breaks TR symmetry, is turned on adiabatically. For this case, the Pfaffian is plotted in Fig. 2e. As the strength of λ_1 increases the positions of the pair of vortices in the upper half-plane of the BZ are modified and move toward the pair in the lower half-plane compared to the Rashba case in Fig. 2d. As we already mentioned before, this trend continues until the vortices disappear at a critical strength $\lambda_1 \approx 3$ before entering the even parity subspace protected by the mirror symmetry. Indeed this corresponds to the boundary in the phase diagram in Fig. 1d of spinless fermions. This observation is consistent with the corresponding degeneracy of edge states as displayed in Fig. 2b. The positions of the four Dirac cones are the direct projection of the vortex positions on the BZ of the edge states in Fig. 2e.

As described above, the Pfaffian $\mathcal{P}(\mathbf{k})$ is a good measure of the topological invariant, even when the Chern number vanishes. It correctly characterizes systems that have a non-trivial band topology due to the mirror symmetry \mathbf{M} . Finally, we can define the mirror topological index by counting the number of vortex cores with the expression

$$I = \frac{1}{2\pi i} \oint_{\partial \mathbf{S}_4} d\mathbf{k} \cdot \nabla_{\mathbf{k}} \log[\mathcal{P}(\mathbf{k})] \mod 2, \quad (4)$$

where $\partial \mathbf{S}_4$ is the boundary of one quarter of the BZ. From the detailed symmetry analysis of phase **II** in the SM, we know that the even parity subspace is along the contour \mathbb{C} . Note that the contour

\mathbb{C} is not a single point, but rather a path which divides the BZ into four independent sections. Since in 2D systems the \mathbf{M} operator connects (k_x, k_y) to $(\pm k_x, \mp k_y)$, similar to the parity operation, and combined with the intrinsic symmetry of the Hamiltonian of phase **II**, namely $\hat{H}_s(\mathbf{k}) = \hat{H}_s(-\mathbf{k})$, the minimal irreducible section becomes one quarter of the BZ. Hence, the odd (even) number of vortices inside a quarter of the BZ determines the nontrivial (trivial) topology of the edge states.

Near the completion of the manuscript, we noticed a different work on the realization of TCIs in a thin-film layers [28], where the 3D mirror symmetry is respected along the film growth direction (mirror plane is perpendicular to the growth direction). In this scenario, the surface states of the film are gapped due to their hybridization with surface states on the opposite side of the sample, although the mirror parity of the wave function on the same surface is an invariant. This is different from our model, where there is no hybridization between surface states in the stacked version of the 2D layers we considered. The mirror symmetry in 2D model is equivalent to π rotational symmetry in 3D with respect to the mirror axes in our model. However, in our case the quasi-2D dispersions and Dirac cones are gapped due to the Coulomb interaction. Thus, the parity of the wave function of the spinful Hamiltonian of phase **II** on the same surface varies due to the oddness/evenness of the mirror symmetries.

CONCLUSIONS

In conclusion, we demonstrated a new path toward realizing non-trivial TCIs through electronic correlations of the Coulomb interaction in 3D compounds with quasi-2D band structure. Specifically, we focused on materials where the ground state orbital orientation of the wave functions order with a 45-degree inter-orbital orientation. Based on a mean-field theory treatment, we identified two topological insulating phases induced by the repulsive Coulomb interaction. It was possible to show that one phase is adiabatically connected to the conventional quantum-spin Hall insulator with a nonzero Chern number; while the other phase is an emergent TCI that is invariant under mirror reflection with an even mirror Chern number, though vanishing Chern number. We introduced a new Z_2 -like mirror topological invariant to capture the band topology of the latter phase by counting the vortex number of the mirror Pfaffian in a quarter of the BZ. Since the discovery of emergent topological phases of band insulators in experiments has not been successful in materials with itinerant bands, our studies open up new directions toward the search of correlation-induced topological phases in real materials with moderate Coulomb interaction in d orbitals at

the surfaces of correlated materials.

Finally, we suggest possible candidates for the emergent TCI phases in materials with crystal field split t_{2g} orbitals that are described by a simple two-orbital effective Hamiltonian, which should be considered as an effective theory for the paramagnetic phase even at finite temperature with normalized parameters.

When the system is a Chern insulator, the anomalous orbital Hall effect with finite magnetic moments will occur due to orbital currents, yet without spin order. Based on this work, we suggest to look for TCIs in the iron-pnictide based nonmagnetic insulators with crystallographic 122 structure [26], where the Fermi surface is close to half-filling. Due to the edge states, the material candidate should show electric conductivity even at low temperature even though the bulk is insulating.

We suggest to focus on pnictides showing paramagnetic and bad metallic conductivity. Based on the experimental evidence [27], the Ni-based compound, BaNi_2As_2 with very low superconducting temperature ($T_c \approx 0.6\text{K}$), is likely such a candidate. It does not show spin-density wave state when the d electron filling is almost fully filled within our two-orbital model. By hole doping with K on the Ba site of BaNi_2As_2 , the electron filling can be reduced to close to half-filled. With compressional stress applied normal to the NiAs layer, the lattice constant in the NiAs layer can be enlarged due to strain responses (see Supplementary Material in Section I). In this regime, a paramagnetic insulating state should be looked into. The BaFe_2As_2 at a temperature above Neel temperature is also a possible area to look for the TCI phase. Other members of the 122 family may also be suitable for detecting the TCI phase but systematic studies are needed to sort this out.

Similar to other TIs, when the topological edge states stacked along the layer growth direction to form the surface states, the surface states can be verified through scanning tunneling and angle-resolved photoemission spectroscopies. In addition, systematic measurements of the Hall conductivity can distinguish the proposed TCI (phase II) from the Chern insulator (phase I), which has the anomalous orbital Hall effect. Moreover, the intrinsic inter-orbital current order should lead to magneto-optical Kerr or Faraday rotation observable in experiments.

ACKNOWLEDGEMENTS

We thank J. Ren, G.-W. Chern and Tanmoy Das for discussions at the initial stages of this work, and especially Fan Zhang for the discussion on mirror symmetry. This work was supported

in part by the Robert A. Welch Foundation under Grant No. E-1146 (Y.-Y.T. and C.S.T.). Work at Los Alamos was supported by the U.S. DOE Contract No. DE-AC52-06NA25396 through the LDRD program (Y.-Y.T., C.-C.J.W.), the Office of Basic Energy Sciences, Division of Materials Sciences and Engineering (M.J.G.), and the Center for Integrated Nanotechnologies, a DOE Basic Energy Sciences user facility (J.-X.Z.). Y.-Y. T. also thanks Los Alamos National Laboratory for its hospitality during his visit.

AUTHOR CONTRIBUTION

Wang and Tai conceived and designed the project, performed the symmetry analysis and identification of topological invariants. Tai performed the numerical band-structure and Chern number calculations. Graf, Zhu, and Ting supervised the project. Tai and Wang wrote the manuscript with contributions from all authors.

ADDITIONAL INFORMATION

Correspondence and requests for materials should be addressed to Y.-Y. Tai and C.-C. Joseph Wang.

-
- [1] Thouless, D. J., Kohmoto, M., Nightingale, M. P. & den Nijs, M. Quantized Hall conductance in a two-dimensional periodic potential. *Phys. Rev. Lett.* **49**, 405 (1982).
 - [2] Haldane, F. D. M. Model for a Quantum Hall Effect without Landau Levels: Condensed-Matter Realization of the "Parity Anomaly". *Phys. Rev. Lett.* **61**, 2015 (1988).
 - [3] Kane, C. & Mele, E. Quantum Spin Hall Effect in Graphene. *Phys. Rev. Lett.* **95**, 226801 (2005); Kane, C. & Mele E. Z_2 Topological Order and the Quantum Spin Hall Effect. *Phys. Rev. Lett.* **95**, 146802 (2005).
 - [4] Knig, M., Weidmann, S., Brune, C., Roth, A., Buhmann, H., Molenkamp, L., Qi, X.-L. & Zhang, S. C. Quantum Spin Hall Insulator State in HgTe Quantum Wells. *Science* **318**, 766 (2007).
 - [5] Bernevig, B. A., T. Hughes, L. & Zhang, S. C. Quantum Spin Hall Effect and Topological Phase Transition in HgTe Quantum Wells. *Science* **314**, 1757 (2006).

- [6] Hsieh, D., Qian, D., Wray, L., Xia, Y., Hor, Y. S., Cava, R. J. & Hasan, M. Z. A topological Dirac insulator in a quantum spin Hall phase. *Nature (London)* **452**, 970 (2008).
- [7] Zhang, H., Liu, C.-X., Qi, X.-L., Dai, X., Fang, Z. & Zhang, S.-C. Topological insulators in Bi_2Se_3 , Bi_2Te_3 and Sb_2Te_3 with a single Dirac cone on the surface. *Nature Physics* **5**, 438 (2009).
- [8] Hasan, M. Z. & Kane, C. L. Topological insulators. *Rev. Mod. Phys.* **82**, 3045 (2010).
- [9] Ando, Y. Topological Insulator Materials. *J. Phys. Soc. Jpn.* **82**, 102001 (2013).
- [10] Klintenberg, M. The search for strong topological insulators. *arXiv*:1007.4838.
- [11] Sun, K., Liu, W. V., Hemmerich, A. & Sarma, S. D. Topological semimetal in a fermionic optical lattice. *Nat. Phys.* **8**, 67-70 (2012).
- [12] Chong, Y. D., Wen, X.-G. & Solijacic, M. Effective theory of quadratic degeneracies. *Phys. Rev. B.* **77**, 235125 (2008).
- [13] Dzero, M., Sun, K., Galitski, V. & Coleman, P. Topological Kondo Insulators. *Phys. Rev. Lett.* **104**, 106408 (2010).
- [14] Hsieh, T. H., Lin, H., Liu, J., Duan, W., Bansil, A., Fu, L. Topological crystalline insulators in the SnTe material class. *Nature Commun.* **3**, 982 (2012).
- [15] Kargarian, M. & Fiete, G. A. Topological Crystalline Insulators in Transition Metal Oxides. *Phys. Rev. Lett.* **110**, 156403 (2013).
- [16] Khomskii, D. I. Role of Orbitals in the Physics of Correlated Electron Systems. *Physica Scripta* **72**, CC8-14 (2005).
- [17] For the single-orbital models of the cuprates, the d -density-wave state [19, 20] breaks the 1-atom per unit cell translational symmetry in addition to the time-reversal symmetry; while the current loop model [21] breaks the time reversal symmetry. In contrast, the two-orbital model presented here does not break the 1-unit cell translational invariance with respect to the inter-orbital current flux order caused by the coupling λ_{AOH}^σ .
- [18] Raghu, S., Qi, X.-L., Honerkamp, C. & Zhang, S.-C. Topological Mott Insulators. *Phys. Rev. Lett.* **100**, 156401 (2008);
- [19] Chakravarty, S., Laughlin, R. B., Morr, D. K. & Nayak, C. Hidden order in the cuprates. *Phys. Rev. B.* **63**, 094503 (2000).
- [20] Zhu, J.-X., Kim, W., Ting, C.S. & Carbotte, J.P. Quasiparticle States around a Nonmagnetic Impurity in a d -Density-Wave State of High- T_c Cuprates. *Phys. Rev. Lett.* **87**, 197001 (2001); Zhu, J.-X. In-plane tunneling spectrum into a [110]-oriented high- T_c superconductor in the pseudogap regime *Phys.*

Rev. B **66**, 104523 (2002).

- [21] Simon, M. E. & Varma, C. M. Detection and Implications of a Time-Reversal Breaking State in Underdoped Cuprates. *Phys. Rev. Lett.* **89**, 247003 (2002).
- [22] Tai, Y.-Y., Zhu, J.-X., Graf, M. J. & Ting, C. S. Calculated phase diagram of doped BaFe₂As₂ superconductor in a C₄-symmetry breaking model. *Europhys. Lett.* **103**, 67001 (2013).
- [23] Chen, H., Tai, Y.-Y., Ting, C. S., Graf, M. J., Dai, J. & Zhu, J.-X. Disorder effects in multiorbital s_±-wave superconductors: Implications for Zn-doped BaFe₂As₂ compounds. *Phys. Rev. B* **88**, 184509 (2013).
- [24] The original model of [3] assumed the 2-Fe per unit cell Hamiltonian. However, a unitary transformation maps the 2-Fe onto the 1-Fe per unit cell model Hamiltonian in the absence of the spin density wave [4].
- [25] Zhang, D. Nonmagnetic Impurity Resonances as a Signature of Sign-Reversal Pairing in FeAs-Based Superconductors. *Phys. Rev. Lett* **103**, 186402 (2009).
- [26] Hoffmann, R. & Zheng, C. Making and breaking bonds in the solid state: the thorium chromium silicide (ThCr₂Si₂) structure. *J. Phys. Chem.* **89**, 4175 (1985).
- [27] Chen, Z. G., Hu, W. Z. & Wang, N. L. Different nature of instabilities in BaFe₂As₂ and BaNi₂As₂ as revealed by optical spectroscopy. *Phys. Stat. Sol.* **247**, 495 (2010).
- [28] Liu, J., Hsieh, T. H., Wei, P., Duan, W., Moodera, J. & Fu, L. Spin-filtered edge states with an electrically tunable gap in a two-dimensional topological crystalline insulator. *Nature Materials* **13**, 178 (2013).
- [29] Teo, J. C. Y., Fu, L. & Kane, C. L. Surface states and topological invariants in three-dimensional topological insulators: Application to Bi_{1-x}Sb_x. *Phys. Rev. B.* **78**, 045426 (2008).

In this Supplementary Material, we provide the additional technical information and details used in the main text of the publication. The following sections contain the in-depth description of the model, numerical calculations, and symmetry analysis:

1. Crystal field splitting of *d* orbitals
2. Mean-field lattice Hamiltonian of correlated electron system
3. Inter-orbital current order of the flux phase
4. Lifting of ground state degeneracy with exchange interaction

5. The Hamiltonian in momentum representation
6. Two types of orbital order with C_{4v} symmetry
7. Vortices as generators of the Berry flux and Chern numbers
8. Symmetry analysis of the time and mirror invariance

CRYSTAL FIELD SPLITTING OF d ORBITALS

For a transition-metal(TM) atom situated in crystal fields due to surrounding ions in compounds, the d atomic levels align differently. The d orbitals include d_{xy} , d_{xz} , d_{yz} , $d_{x^2-y^2}$, and d_{z^2} . In a spherical crystal field, the d orbitals are all degenerate. For a TM atom caged by four ligand atoms, a tetrahedral crystal field splits the five d orbitals into t_{2g} and e_g manifolds where t_{2g} levels are higher in energy. With a tetragonal crystal field distortion introduced by anisotropic strains or effective strains with different types of the surrounding ligand atoms, part of the degeneracy of the t_{2g} orbitals is lifted with the d_{xy} level energetically separated from d_{xz} and d_{yz} orbitals which are the relevant degrees of freedom we are interested in. The d_{xy} level will be higher in energy when the strain is stretched along the z axis and vice versa as shown in Fig. (3).

MEAN-FIELD LATTICE HAMILTONIAN OF CORRELATED ELECTRON SYSTEM

In this section, we derive the mean-field form of the Coulomb interaction. The Hamiltonian of interest is $H^s = H^0 + H^U + H^J + H^V$, where the superscript s indicates that we include the spin degrees of freedom. In real-space the lattice Hamiltonian is given by

$$\begin{aligned}
H^0 &= \sum_{IJ,\alpha\beta,\sigma} (t_{IJ}^{\alpha\beta} - \mu \delta_{IJ} \delta_{\alpha\beta}) c_{I\alpha,\sigma}^\dagger c_{J\beta,\sigma}, \\
H^U &= U \sum_{I,\alpha,\sigma} n_{I\alpha,\sigma} n_{I\alpha,\sigma'}, \\
H_h^J &= U' \sum_{I\sigma\alpha} n_{I\alpha,\sigma} n_{I\bar{\alpha},\sigma'} + (U' - J_h) \sum_{I\sigma\alpha} n_{I\alpha,\sigma} n_{I\bar{\alpha},\sigma}, \\
H^V &= \sum_{I \neq J, \alpha \neq \beta, \sigma} V_{IJ}^{\alpha\beta} n_{I\alpha,\sigma} n_{J\beta,\sigma},
\end{aligned} \tag{5}$$

where $U' = U - 2J_h$. Here H^0 is the kinetic term describing the hopping of electrons in the 1-Fe per unit cell formulation.[3, 4] In our two-orbital model with $\alpha, \beta = (1, 2)$ the non-zero hopping

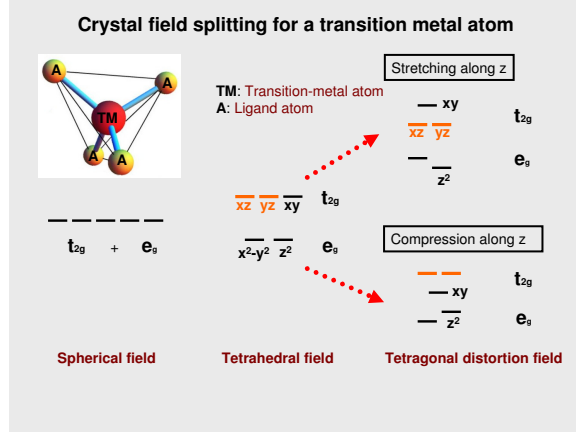


FIG. 3: **Crystal field splitting.** In a spherical crystal field, five d orbitals including d_{xy} , d_{xz} , d_{yz} , $d_{x^2-y^2}$, and d_{z^2} are degenerate. With a tetrahedral crystal field, the five d orbitals into t_{2g} and e_g manifolds where t_{2g} levels are higher in energy. With a tetragonal crystal field distortion, part of the degeneracy of the t_{2g} orbitals is lifted with the d_{xy} level energetically separated from d_{xz} and d_{yz} orbitals. When the strain is stretched (compressed) along the layer growth direction, the wave function overlaps between d_{xz} and d_{yz} orbitals are reduced (enhanced) causing the reduction (enhancement) in Coulomb interaction. Therefore, d_{xz} and d_{yz} are lower (higher) in energies.

parameters are chosen to describe the generic pnictide BaFe_2As_2 for purpose of illustration,

$$\begin{aligned}
 t_1 &= t_{\pm\hat{x}}^{\alpha\alpha} = t_{\pm\hat{y}}^{\alpha\alpha} = 0.09, \\
 t_2 &= t_{\pm(\hat{x}-\hat{y})}^{11} = t_{\pm(\hat{x}+\hat{y})}^{22} = 0.08, \\
 t_3 &= t_{\pm(\hat{x}+\hat{y})}^{11} = t_{\pm(\hat{x}-\hat{y})}^{22} = 1.35, \\
 t_4 &= t_{\pm(\hat{x}\pm\hat{y})}^{\alpha\bar{\alpha}} = -0.12, \\
 t_5 &= t_{\pm\hat{x}}^{\alpha\bar{\alpha}} = t_{\pm\hat{y}}^{\alpha\bar{\alpha}} = -1, \\
 t_6 &= t_{\pm 2\hat{x}}^{\alpha\alpha} = t_{\pm 2\hat{y}}^{\alpha\alpha} = 0.25.
 \end{aligned} \tag{6}$$

The interaction part is captured by the terms H^U and H^J , which are the on-site intra-orbital *Hubbard interaction* and *Hund's coupling*, as well as the term H^V , which is the inter-orbital ($\alpha \neq \beta$) *Coulomb* interaction between lattice sites I and J . Note that we also considered intra-orbital offsite Coulomb interaction ($\alpha = \beta$), but found no interesting topological phases. Thus, we will not further consider the intra-orbital interaction in the current work. By investigating H^U and H^V in the mean-field approximation, we can test whether there exist new and anomalous ground states due to the inter-orbital Coulomb interaction, although the incorporation of quantum

$I \setminus J$	$I \pm \hat{x}, d_{xz}$	$I \pm \hat{x}, d_{yz}$	$I \pm \hat{y}, d_{xz}$	$I \pm \hat{y}, d_{yz}$
I, d_{xz}	0	1	0	-1
I, d_{yz}	-1	0	1	0

TABLE I: The matrix elements of $\epsilon_{\alpha\beta}^{IJ}$ preserve the translational invariance of the 1-Fe per unit cell and the C_{4v} point group symmetry.

fluctuations may change the details of such a phase diagram. For the on-site inter-orbital H^U we write in standard mean-field approximation

$$H^U = U \sum_{I\alpha, \sigma \neq \sigma'} \langle n_{I\alpha\sigma} \rangle n_{I\alpha\sigma'}. \quad (7)$$

On the other hand, we have at least two possibilities for the inter-orbital H^V to decouple the fermionic operators within mean-field theory, namely $H^V = H^{CDW} + H^{AOH}$, where

$$\begin{aligned} H^{CDW} &= \sum_{I \neq J, \alpha \neq \beta, \sigma} V_{IJ} \langle n_{I\alpha\sigma} \rangle n_{J\beta\sigma}, \\ H^{AOH} &= - \sum_{I \neq J, \alpha \neq \beta, \sigma} V_{IJ} \langle c_{I\alpha, \sigma}^\dagger c_{J\beta, \sigma} \rangle c_{J\beta, \sigma}^\dagger c_{I\alpha, \sigma}. \end{aligned} \quad (8)$$

In this work, we simplify the Coulomb coupling and include only the nearest-neighbor (NN) interaction with $V_{\langle ij \rangle} = V_1$. In the 2D-periodic calculation of the bulk material, the CDW term is not a stable ground state and only H^{AOH} has a stable solution at a finite value of $V_1 \gtrsim 1.6$, see Fig. 4. Unlike Bardeen-Cooper-Schrieffer (BCS) theory, where any non-zero pairing strength will lead to superconductivity, here a threshold has to be overcome to induce long-range orbital order. Naturally, this makes it more challenging to find materials with orbital-ordered ground states. We also checked numerically for magnetism and found that a Hubbard term with $U = 3.2$ and $V_1 \gg J$ does not induce long-range magnetic order in our simple, low-energy two-orbital model. For the rest of this work, we consider the region of the interaction $V_1 - J$ phase diagram where no magnetic order emerges.

INTER-ORBITAL CURRENT ORDER OF THE FLUX PHASE

Here, let us define the mean-field inter-orbital current order parameter of the flux phase due to the anomalous orbital Hall term H^{AOH} ,

$$\chi_{\alpha\beta, \sigma}^{IJ} \equiv V_1 \langle c_{I\alpha, \sigma}^\dagger c_{J\beta, \sigma} \rangle. \quad (9)$$

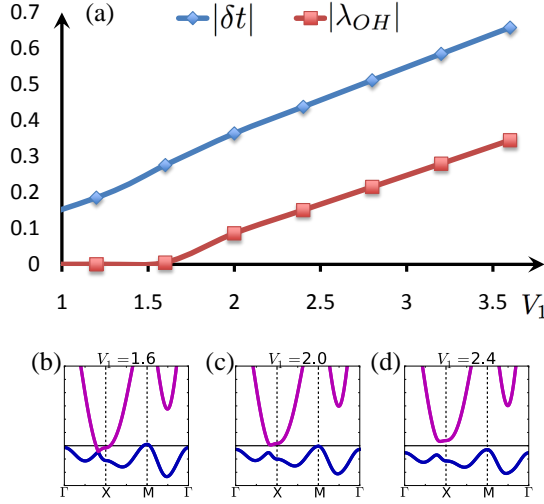


FIG. 4: (a) The mean-field order parameter of the H^{AOH} term, where $\delta t/\lambda_{AOH}$ are the real/imaginary part of the order parameter. (b),(c) and (d) The evolution of the dispersion of the electronic band structure for the 1-Fe/unit cell along high-symmetry directions in the BZ for different interaction strengths of V_1 .

The mean-field calculated nearest-neighbor order parameter $\chi_{\alpha\beta,\sigma}^{IJ}$ is a complex number with real and imaginary parts, $\chi_{\alpha\beta,\sigma}^{IJ} = \delta t + i\epsilon_\sigma \epsilon_{\alpha\beta}^{IJ} \lambda_{AOH}$, where we define,

$$\begin{aligned} \delta t &= -|\text{Re } \chi_{\alpha\beta,\sigma}^{IJ}|, \\ \lambda_{AOH} &= |\text{Im } \chi_{\alpha\beta,\sigma}^{IJ}|. \end{aligned} \quad (10)$$

Note that the first term, δt , is always negative and homogeneous in real space. It will contribute to H^0 to its NN inter-orbital hopping term t_5 [4]. The second term, λ_{AOH} , is the generator of the anomalous orbital Hall effect, which is of key interest in this work. Consequently, the term H^{AOH} can be rewritten in a more compact form,

$$H^{AOH} = i\epsilon_\sigma \lambda_{AOH} \sum_{IJ, \alpha \neq \beta, \sigma} \epsilon_{\alpha\beta}^{IJ} c_{I\alpha,\sigma}^\dagger c_{J\beta,\sigma}, \quad (11)$$

where $\epsilon_\sigma = \epsilon_{\uparrow/\downarrow} = \pm 1$ and the elements of the tensor $\epsilon_{\alpha\beta}^{IJ}$ are expressed in Table. I and the real part of H^{AOH} has been absorbed into the NN inter-orbital hopping terms, $t_5 \rightarrow t_5 + \delta t$. Figure 4(b) shows that the Fermi surface is shifted downward at the Γ and M points, due to the contribution of δt alone. Once the imaginary part λ_{AOH} is included, the degeneracy of the bulk Dirac cone near the X point in the Brillouin zone (BZ) is lifted immediately, as shown by the opening of a gap in Fig. 4(c). The gap increases with increasing value of λ_{AOH} as further shown in Fig. 4(d).

LIFTING OF GROUND STATE DEGENERACY WITH EXCHANGE INTERACTION

In the main text, we have shown that without introducing other terms, the ground state of H^{AOH} leads to two degenerated phases, namely $\epsilon_{\uparrow} = \pm\epsilon_{\downarrow}$. In order to discuss the possibility of lifting this degeneracy, we introduce a perturbation caused by considering one additional term of the Hund's coupling type to Eq. (5), as discussed by Sano[2], $H^J \rightarrow H^J + H_2^{J_h}$.

$$H_2^{J_h} = -J_h \sum_{I\alpha} (c_{I,\alpha,\uparrow}^\dagger c_{I,\alpha,\downarrow} c_{I,\bar{\alpha},\downarrow}^\dagger c_{I,\bar{\alpha},\uparrow} + h.c.). \quad (12)$$

Then we have the mean-field decoupled Hamiltonian $H_2^{J_h}$,

$$H_2^{J_h} = \lambda_{J_h} \sum_{I\alpha} (c_{I,\alpha,\uparrow}^\dagger c_{I,\alpha,\downarrow} + c_{I,\bar{\alpha},\downarrow}^\dagger c_{I,\bar{\alpha},\uparrow} + h.c.), \quad (13)$$

where the mean-field order parameter λ_{J_h} is defined as $\lambda_{J_h} = -J_h \langle c_{I,\alpha,\sigma}^\dagger c_{I,\alpha,\bar{\sigma}} \rangle$. Finally, if we insert Eq. (13) into the Hamiltonian H and manually assign a real value to λ_{J_h} , we can confirm that phase **II** with $\epsilon_{\uparrow} = -\epsilon_{\downarrow}$ is the preferred ground state for any small λ_J .

THE HAMILTONIAN IN MOMENTUM REPRESENTATION

In this section, we Fourier transform H^s into \mathbf{k} -space for the 1-Fe per unit cell with the mean-field calculated order parameter λ_{AOH} and the manually added terms λ_0 and λ_1 . For pedagogical reasons, we focus first on the spin polarized Hamiltonian for the spin component σ , $H = \frac{1}{N} \sum_k \psi_k^\dagger \hat{H} \psi_k$, where $\psi_k = (c_{k,1}, c_{k,2})^T$ and c_1/c_2 stand for annihilating electrons on d_{xz}/d_{yz} orbitals. In \mathbf{k} -space the Hamiltonian is conveniently written as

$$\hat{H}(\epsilon_\sigma) = E_0 + \vec{B} \cdot \vec{\tau}, \quad (14)$$

where $\vec{B} = (X, Y, Z)$ and $\vec{\tau}$ is the vector of Pauli matrices spanning the orbital $SU(2)$ space with

$$\begin{aligned} E_0 &= 2t_1 [\cos(k_x) + \cos(k_y)] + 2t_6 [\cos(2k_x) + \cos(2k_y)], \\ &+ 2(t_2 + t_3) [\cos(k_x) \cos(k_y)] - \mu, \\ X &= 4t_4 [\cos(k_x) \cos(k_y)] + 2(t_5 + \delta t) [\cos(k_x) + \cos(k_y)], \\ Y &= 2\epsilon_\sigma \lambda_{AOH} [\cos(k_x) - \cos(k_y)] + \lambda_1, \\ Z &= 2(t_2 - t_3) [\sin(k_x) \sin(k_y)] + \lambda_0. \end{aligned} \quad (15)$$

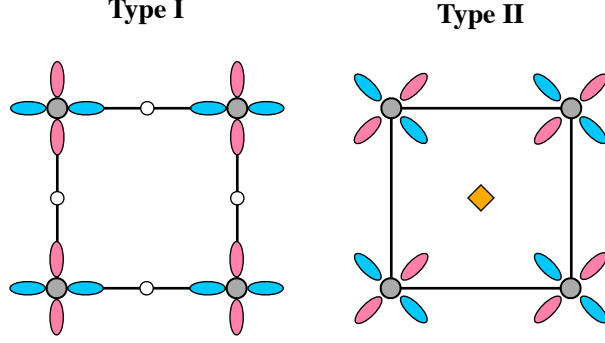


FIG. 5: **Orbital order.** Two types of orbital in a lattice with C_{4v} symmetry. Type I (left panel), the orbital orientation along the NN bond direction. Type II (right panel), the orbital orientation along the next-nearest neighbor (NNN) bond direction. The blue (red) colored lobes represent the d_{xz} (d_{yz}) orbitals of the Fe atoms (filled gray circles). The filled yellow diamond in the right panel indicates the anion atom, which prefers the Type II orbital locking in the Fe-only effective model.

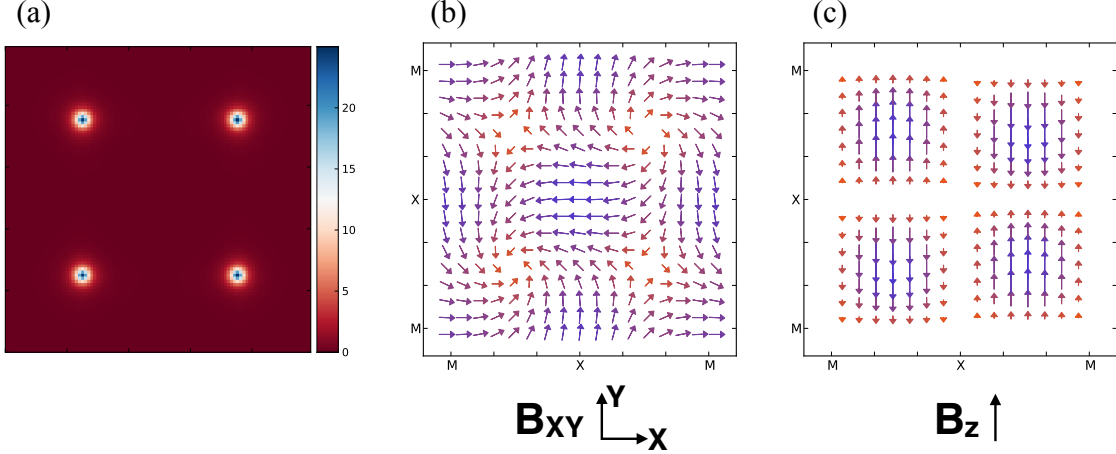


FIG. 6: **Berry curvature and generalized magnetic field \vec{B} .** (a) Color-map image of the Berry curvature of the simplified spinless Hamiltonian $\tilde{H}(\mathbf{k})$ in the BZ. (b) and (c) The components of the complex auxiliary vector field $\vec{B} = (X, Y, Z)$ of $\tilde{H}(\mathbf{k}) = \tilde{E}_0 + \vec{B} \cdot \vec{\tau}$. Each vector $B_{xy} = (B_x, B_y)$ with color-map red (small) to blue (large).

In the 2×2 matrix notation we can write specifically

$$\hat{H}(\epsilon_a) = \begin{pmatrix} E_0 + Z, & X - iY \\ X + iY, & E_0 - Z \end{pmatrix}. \quad (16)$$

Note that Eq. (16) has been used in the main text for the calculation of the Chern number.

We close this section by expanding the formulation of the spinless Hamiltonian to include spin

degrees of freedom. The enlarged spin-orbital space becomes $SU(2) \times SU(2)$ or $\vec{\tau} \otimes \vec{\sigma}$. In such a notation, a Rashba spin-orbital coupling term enters on the off-diagonal entries of the 4×4 matrix,

$$\hat{H}_s = \begin{pmatrix} \hat{H}(\epsilon_\uparrow = 1), & i\lambda_R \sigma_z \\ -i\lambda_R \sigma_z, & \hat{H}(\epsilon_\downarrow = -1) \end{pmatrix}. \quad (17)$$

Note that Eq. (17) has been used in the main text to calculate the mirror symmetry properties of the topological crystalline phase.

TWO TYPES OF ORBITAL ORDER LOCKED IN A LATTICE WITH C_{4v} SYMMETRY

As shown in Fig. 5 the lattice with C_{4v} symmetry allows two different types of orbital order. The second type can generate Dirac cones along the Γ - X direction in the bulk dispersion. In what follows, we focus on the \mathbf{k} -dependent inter-orbital hopping energies with C_{4v} symmetry,

$$H^{xz,yz} = \sum_k [\epsilon_{xz}(k) c_{xz,k}^\dagger c_{xz,k} + \epsilon_{yz}(k) c_{yz,k}^\dagger c_{yz,k} + \dots], \quad (18)$$

with

$$\begin{aligned} \epsilon_{xz} &= -2t \cos(\mathbf{k} \cdot \vec{a}_1), \\ \epsilon_{yz} &= -2t \cos(\mathbf{k} \cdot \vec{a}_2), \end{aligned} \quad (19)$$

where $\vec{a}_{1,2}$ are orthogonal to each other and indicate the bond direction of the effective hopping term t . If we choose $\vec{a}_1 = (1, 0)$ and $\vec{a}_2 = (0, 1)$, then this corresponds to type-I order with C_{4v} symmetry. On the other hand, for $\vec{a}_1 = (1, 1)$ and $\vec{a}_2 = (-1, 1)$ it becomes

$$\hat{H}^{xz,yz} = -2t [\cos(k_x) \cos(k_y) + \tau_z \sin(k_x) \sin(k_y)], \quad (20)$$

which gives rise to the τ_z term in the spinless Hamiltonian in Eq. (16).

VORTICES AS GENERATORS OF THE BERRY FLUX AND CHERN NUMBERS

The anomalous orbital Hall effect of the spinless Hamiltonian with Chern number $\mathcal{C} = \pm 2$ is the combined effect of functions X , Y and Z . The Chern number can be calculated directly through the area integration of the Berry curvature[10]

$$\Omega(\mathbf{k})^\pm = i \frac{\langle \pm | \frac{\partial \hat{H}(k)}{\partial k_x} | \mp \rangle \langle \mp | \frac{\partial \hat{H}(k)}{\partial k_y} | \pm \rangle - (k_x \leftrightarrow k_y)}{(E_\pm - E_\mp)^2}. \quad (21)$$

In viewing the symmetry of \vec{B} , we know that the Dirac cones can be re-defined by taking any two components of (X, Y, Z) . To be specific, let us consider the simplified spinless Hamiltonian in Eq. (15) with interaction renormalized coefficients,

$$\begin{aligned}\tilde{E}_0 &= 0, \\ \tilde{X} &= t^x (4 t^4 [\cos(k_x) \cos(k_y)] + 2 t^5 [\cos(k_x) + \cos(k_y)]), \\ \tilde{Y} &= t^y (2 \lambda_{AOH} [\cos(k_x) - \cos(k_y)]), \\ \tilde{Z} &= t^z (2 (t_2 - t_3) [\sin(k_x) \sin(k_y)]).\end{aligned}\tag{22}$$

Here \tilde{E}_0 can be regarded as a rigid energy shift and does not contribute to the calculation of the topological invariant. In the main text, four Dirac cones are generated in the bulk bands with renormalized hopping parameters $t^{x,y,z} = (1, 0, 1)$, where the band energy becomes $E_{\pm}^{1,0,1}(\mathbf{k}) = \pm \sqrt{\tilde{X}^2 + \tilde{Z}^2}$. The four Dirac cones are located around the M point of the BZ, satisfying the criterion $\tilde{X}^2 + \tilde{Z}^2 = 0$. A key result of this work is that a non-zero function \tilde{Y} is a necessary but not sufficient condition for a topological ground state. It can be viewed as a perturbation where the massless fermions acquire mass and a gap opens at the Dirac cones. Here, if we choose the parameters $t^{x,y,z} = (1, 1, 0)$, then the dispersion becomes $E_{\pm}^{1,1,0}(\mathbf{k}) = \pm \sqrt{\tilde{X}^2 + \tilde{Y}^2}$, and the Dirac cones are located in the BZ at $(\pm \frac{\pi}{2}, \pm \frac{\pi}{2})$ and $(\pm \frac{\pi}{2}, \mp \frac{\pi}{2})$. In addition, when we turn on a small t^z or \tilde{Z} , then the degeneracy at the Dirac cones is lifted and the calculated Chern number becomes ± 2 for each band. The corresponding Berry curvature is shown as a color-map image in Fig. 6(a), where four high intensity spots can be found at the positions of the Dirac cones. If we regard these four Dirac cones as topological defects of a *generalized* magnetic field \vec{B} in the Hamiltonian acting on the pseudo-spin degrees of freedom, that is, $\vec{B} \cdot \vec{\tau}$, where $\vec{B} = (\tilde{X}, \tilde{Y}, \tilde{Z})$, then it is rather straightforward to map out the B_{xy} (in-plane) and B_z (out-of-plane) components in Figs. 6(b) and (c). Knowing these two-dimensional (2D) vector maps, one can graphically solve for the Chern number by mapping the vector \vec{B} around each singularity onto the Bloch sphere, following the procedure outlined by Bernevig [5]. Thus the \vec{B} -field winding around each topological defect (Dirac cone) contributes the winding number $2\pi \times \frac{1}{2} = \pi$, where the factor one-half stems from the spin $\frac{1}{2}$. Hence the spinless Hamiltonian has the total Chern number $\mathcal{C} = \pm(4 \times \pi)/2\pi = \pm 2$.

SYMMETRY ANALYSIS OF THE TIME AND MIRROR INVARIANCE

In this section, we discuss the symmetry classification of phases **I** and **II** of the spinful Hamiltonian with spin degrees of freedom. A detailed account of the symmetry operators used in the main text is given. The spinful Hamiltonian in \mathbf{k} -space of fermions is defined by $H^s = \phi_{\mathbf{k}}^\dagger \hat{H}_s(\mathbf{k}) \phi_{\mathbf{k}}$, where $\phi_{\mathbf{k}} = (c_{\mathbf{k},1\uparrow}, c_{\mathbf{k},2\uparrow}, c_{\mathbf{k},1\downarrow}, c_{\mathbf{k},2\downarrow})^T$. We re-write \hat{H}_s as a direct tensor product of Pauli matrices in the combined orbital pseudo-spin and spin spaces, $\hat{H}_s^{I,II} = X \tau_x \otimes I + Z \tau_z \otimes I + \hat{H}_{AOH}^{I,II}$, where the orbital flux term, $\hat{H}_{AOH}^{I,II}$, of phases **I** and **II** is either $\hat{H}_{AOH}^I = Y \tau_y \otimes I$ or $\hat{H}_{AOH}^{II} = Y \tau_y \otimes \sigma_z$. Here I is the 2×2 unity matrix in spin space.

Intrinsic inversion symmetry and TR symmetry violation of spinless \hat{H}

We start our symmetry analysis by noting that the quasi-2D Hamiltonian of spinless fermions, \hat{H} , in a tetragonal system has intrinsic inversion symmetry $\hat{H}(\mathbf{k}) = \hat{H}(-\mathbf{k})$. This corresponds to a 180° rotation in the k_x - k_y plane. Moreover, for the spinless Hamiltonian the time-reversal (TR) operator is given by the charge conjugation operator, $\mathbf{T} = \mathbf{K}$, and satisfies the relation

$$\begin{aligned} \mathbf{T} \hat{H}[\lambda_{AOH}](\mathbf{k}) \mathbf{T}^{-1} &= \hat{H}[-\lambda_{AOH}](-\mathbf{k}) \\ &= \hat{H}[-\lambda_{AOH}](\mathbf{k}), \end{aligned} \quad (23)$$

which tells us that the TR symmetry is violated, because it reverses the orbital current direction from $\lambda_{AOH} \rightarrow -\lambda_{AOH}$.

Parity or mirror invariance of spinless \hat{H}

In addition to the inversion symmetry, the spinless quasi-2D Hamiltonian is invariant under mirror reflections. The two mirror axes x and y obey the parity operation

$$\mathbf{P} \hat{H}(k_x, k_y) \mathbf{P}^{-1} = \hat{H}(\pm k_x, \mp k_y), \quad (24)$$

respectively, with $\mathbf{P} = \tau_x \mathbf{K}$. This statement is universally true for our model Hamiltonians and applies also to phases **I** and **II** of the spinful Hamiltonian. Note that in 2D the parity operation is a mirror reflection, which flips the sign of only one coordinate, otherwise it would be a rotation.

Parity and mirror invariance of phase II of spinful \hat{H}_s

The spinful Hamiltonian for fermions with spin degrees of freedom satisfies similar symmetry operations as before. However, now we need to pay attention to the fact that the mirror and TR operators flip the spin of the fermion and must be defined in the enlarged $SU(2) \otimes SU(2)$ space as $\mathbf{M} = \tau_x \otimes (-i\sigma_y)$ and $\mathbf{T} = \hat{1} \otimes (-i\sigma_y \mathbf{K})$, where $\hat{1}$ is the unity matrix in orbital space. Then, the generalized mirror symmetry \mathbf{M} is equivalent to the parity symmetry \mathbf{P} of the spinless fermion. To summarize the key results of our symmetry analysis, our spinful model Hamiltonian of phase **II** is invariant under each of the TR- and mirror (parity) operations:

$$\mathbf{T} \hat{H}_s^{II}(\mathbf{k}) \mathbf{T}^{-1} = \hat{H}_s^{II}(-\mathbf{k}) = \hat{H}_s^{II}(\mathbf{k}), \quad (25)$$

$$\mathbf{M} \hat{H}_s^{II}(k_x, k_y) \mathbf{M}^{-1} = \hat{H}_s^{II}(\pm k_x, \mp k_y). \quad (26)$$

Even and odd parity subspaces of phase II of spinful \hat{H}_s

For the spinful Hamiltonian, the Chern number is only meaningful for phase **I**. This can be seen from its non-zero Chern number $\mathcal{C}[\hat{H}_s^I] = -\mathcal{C}[\mathbf{M} \hat{H}_s^I \mathbf{M}^{-1}] = -\mathcal{C}[\mathbf{T} \hat{H}_s^I \mathbf{T}^{-1}] = \pm 4$. Consequently, \hat{H}_s^I has two distinguishable degenerated states of $\mathcal{C} = \pm 4$, which can be mapped onto each other.

On the other side, phase **II** also has two distinguishable degenerated states, however, these two states cannot be distinguished by the Chern number, because $\mathcal{C}[\hat{H}_s^{II}] = 0$. Thus, we need to further examine its symmetry properties to see whether it is topological or not. A very direct and useful check is to see whether the system has a Z_2 -like invariant index. This symmetry has been widely used in the search for 2D and 3D topological insulators, because there exist general methods to calculate the Z_2 topological invariant, especially when the Hamiltonian exhibits inversion symmetry.[6–9] In phase **II**, the operator \mathbf{M} commutes with the orbital-flux term \hat{H}_{AOH}^{II} and \hat{H}_s^{II} . The even parity subspace is described along the contour, $\mathbb{C} \in \{(\Gamma - M); (M - X)\}$, and gives the commutation relation, $\mathbf{M} \hat{H}_s^{II}(\mathbb{C}) \mathbf{M}^{-1} = \hat{H}_s^{II}(\mathbb{C})$. Whereas the odd parity subspace is located at the high-symmetry points for the parameters we choose, $\Lambda_n \in \{(\pm \frac{\pi}{2}, \pm \frac{\pi}{2}); (\pm \frac{\pi}{2}, \mp \frac{\pi}{2})\}$, and gives the anti-commutation relation, $\mathbf{M} \hat{H}_s^{II}(\Lambda_n) \mathbf{M}^{-1} = -\hat{H}_s^{II}(\Lambda_n)$. This \pm -parity symmetry motivated us to construct the Z_2 -like topological invariant in the main text in order to test for the topological ground state with vanishing Chern number.

-
- [1] T. Zhou, D. Zhang and C. S. Ting, *Spin-density wave and asymmetry of coherence peaks in iron pnictide superconductors from a two-orbital model*, Phys. Rev. B **81**, 052506 (2010).
 - [2] K. Sano and Y. Ono, *Ferromagnetism and superconductivity in the multi-orbital Hubbard model: Hund's rule coupling versus crystal-field splitting*, J. Phys. Soc. Jpn. **72**, 1847 (2003).
 - [3] Y.-Y. Tai, J.-X. Zhu, M. J. Graf, and C. S. Ting, *Calculated phase diagram of doped BaFe₂As₂ superconductors in a C₄-symmetry breaking model*, Europhys. Lett. **103**, 6700 (2013).
 - [4] H. Chen, Y.-Y. Tai, C. S. Ting, M. J. Graf, Jianhui Dai, and J.-X. Zhu, *Disorder effects in multiorbital s^{\pm} -wave superconductors: Implications for Zn-doped BaFe₂As₂ compounds*, Phys. Rev. B **88**, 184509 (2013).
 - [5] B. Andrei Bernevig and Taylor L. Hughes, *Topological Insulators and Topological Superconductors*, Princeton University Press, Princeton (2013).
 - [6] L. Fu, C. L. Kane, and E. J. Mele, *Topological invariants of time-reversal-invariant band structures*, Phys. Rev. Lett. **98**, 106803 (2007).
 - [7] J. E. Moore and L. Balents, *Topological invariants of time-reversal-invariant band structures*, Phys. Rev. B **75**, 121306 (2007).
 - [8] R. Roy, *Topological phases and the quantum spin Hall effect in three dimensions*, Phys. Rev. B **79**, 195322 (2009).
 - [9] L. Fu and C. L. Kane, *Topological insulators with inversion symmetry*, Phys. Rev. B **76**, 045302 (2007).
 - [10] D. Xiao, M.-C. Chang, and Q. Niu, *Berry phase effects on electronic properties*, Rev. Mod. Phys. **82**, 1959 (2010).